

Nonequilibrium Force-Flow Relations in Networks

Ying-Jen Yang^{1,*} and Ken A. Dill^{1,2,3,†}

¹*Laufer Center of Physical and Quantitative Biology, Stony Brook University*

²*Department of Physics, Stony Brook University*

³*Department of Chemistry, Stony Brook University*

In a companion paper [1], we outlined a general theory for nonequilibrium (NEQ) network statistical physics, *Caliber Force Theory*, (CFT). It resembles the “First and Second Laws” basis of Equilibrium (EQ) Thermodynamics, except that dynamics requires maximization of *path entropy* ($\mathcal{S}_{\text{path}}$), not *state entropy*. Here, we elaborate the mathematics of the forces ($d\mathcal{S}_{\text{path}}/dx$), the fluctuation-respond relations, and the Maxwell-Onsager-like symmetry relations. And we give applications beyond thermal baths—such as networks in ecology, biochemistry, vehicle traffic, and other force-flow networks. Beyond past work on inequalities, it gives equalities; and it gives forces, which allows for studies of optimization, conflicts, congestion and network design; and it gives a third Kirchhoff-like relation that applies to networks that have fluctuating flows.

A Two Laws approach to theories of nonequilibrium forces and flows. We consider general network state spaces of nodes and edges. Some mobile agents flow along the edges probabilistically and can dwell on the nodes. The aim is to predict force-flow relationships. Historically, the search for principles of Non-Equilibrium (NEQ) has started from the “Two-Laws” framework of Equilibrium (EQ) Thermodynamics: a First Law of conservation (which, for dynamics, refers to the flowing agents at each time point); and a Second Law of variational principle (which, for dynamics, gives forces to vary the statistics of a process). In a companion paper [1], we present a Two-Laws theory for NEQ, which we call *Caliber Force Theory*. Here, we give the math details, procedures, and some illustrative applications. Much of the universe of today’s force-flow modeling of stochastic processes falls into three categories:

(1) First Law alone, just conservation: This includes Master equations, Markov processes, and Fokker-Planck equations, which relate time-dependent node distributions to transition rates for a given network state space [2, 3]. These models apply arbitrarily Far From Equilibrium (FFE), to fast flows as well as slow ones. These treatments require no notion of forces and no dynamical variational principle resembling the Second Law for equilibria.

(2) First Law plus local-EQ forces, *Stochastic Thermodynamics* (ST): This approach combines such First-Law modeling with forces that are defined by principles of equilibrium thermodynamics. These forces are the free energy differences of fast-equilibrating reservoirs that acquire properties of dynamical directionality (cycle affinity) through the Arrhenius relation [4–7]. In practical terms, what approach (2) introduces, beyond just (1) above, is an assumed relationship of transition rates to energies, such as

$$\text{rate} = e^{\text{energy}/k_{\text{B}}T}, \quad (1)$$

where $k_{\text{B}}T$ is the Boltzmann constant times temperature of the EQ bath. Stochastic rate models that contain factors

of $k_{\text{B}}T$, such as Einsteinian diffusion, Arrhenius kinetics, Rouse-Zimm polymer dynamics and Langevin modeling, fall into this category. This category (2) is premised on a Local Detailed Balanced (LDB) assumption. In this category, dynamical distributions are not derived from a principle and a model as they would be for deriving the Boltzmann Distribution of EQ statistical physics; rather, rate distributions under LDB are assumed to be the local-EQ fluctuations from contact with the controlling reservoirs.

The need for a principled definition of force for non-equilibria. EQ physics derives its definitions of forces through a variational principle, the Second Law of Thermodynamics. EQ problems begin from a complete set of observables, such as $\mathbf{x} = (U, V, N)$. They then derive their corresponding forces ($1/T, P/T, -\mu/T$) from the maximization of entropy over the accessible states, dS_{state}/dx . What then drives the flows—i.e. changes from a prior EQ to a new EQ—are the differences of $(T, P, -\mu)$ from a driver to a receiver reservoir.

In contrast, *forces* in NEQ are typically defined in a more *ad hoc* way, often based on whatever control variable changes a flow in monotonic proportion, linearly or nonlinearly. For example, the flow of particles of concentration $c(x)$ as a function of a coordinate x , is given by Fick’s Law, $\langle J \rangle = -D\partial c(x)/\partial x$, where D is the diffusion coefficient. But, if you take the force in this case to be the gradient of $c(x)$, then this is not conceptually the same as assuming the local equilibrium force, $\Delta\mu(x) = -k_{\text{B}}T \ln c(x)$. Similarly, for Fourier’s law of heat flow, the force can be taken as the gradient of temperature, $\partial T(x)/\partial x$, but this differs from the local equilibrium force, which is $1/T$. Most relevant here—for networks having net fluxes J with rates k_{ij} and node populations π_i —are the following expressions based on the entropy production rate (EPR), which takes several equivalent forms for nonequilibrium steady states [4, 5, 8–10]:

$$\text{EPR} = \sum_{i < j} J_{ij} \ln \frac{k_{ij}}{k_{ji}} \quad (2a)$$

$$= \sum_{i < j} J_{ij} \ln \frac{\pi_i k_{ij}}{\pi_j k_{ji}} = \sum_{\text{cycle}, c} J_c \ln \frac{k_{i_0 i_1} k_{i_1 i_2} \dots k_{i_{\sigma} i_0}}{k_{i_{\sigma} i_1} \dots k_{i_2 i_1} k_{i_1 i_0}} \quad (2b)$$

* ying-jen.yang@stonybrook.edu

† dill@laufercenter.org

where cycle c has a state sequence $i_0 i_1 i_2 \dots i_\sigma i_0$, J_{ij} is the net flow on edge ij , and J_c is the cycle flux. Schnakenberg called both logarithmic terms in Eqs. (2b) forces [4]. Hill considered the cycle affinities—the log term on the right of Eq. (2b)—to be the driving forces of NEQ [5]. And, others called $\ln(k_{ij}/k_{ji})$ forces [11, 12]. The present work was motivated by the need for a more principled notion of nonequilibrium forces, based on the same Two-Law derivation and equipped with conjugated relations as in EQ.

(3) First Law plus arbitrary NEQ forces. In the companion to the present paper [1], we have shown that a complete set of dynamical variables for stochastic dynamics on a network is \mathbf{x} = (node populations π_n , edge traffic τ_{ij} , and cycle flux J_c), defined below. We obtain the NEQ forces by maximizing the path entropy, $d\mathfrak{S}_{\text{path}}/d\mathbf{x}$, according to the principle of Maximum Caliber [13–16]. We show how this Two-Laws formulation of dynamics, just like the Two-Laws formulation of equilibria, leads to a zoo of rigorous relationships that give fluctuation formulae and Maxwell-and-Onsager-like symmetry relations. Also, it readily generalizes to non-Markovian systems. Here we give the mathematical details and some applications.

Comparison to other Nonequilibrium Theories. Past efforts have not led to a complete Two-Laws theory (see [1] and Discussion section below). On the one hand, ST provides many useful relations about the fluctuations and time irreversibility of stochastic dynamics [4, 7, 17–21], but it lacks the Second-Law-like variational principle basis for deriving forces and conjugate relations between observables and forces [22, 23]. On the other hand, the value of Max Cal, and its equivalent exponential tilting in Large Deviation Theory [24–27], is that it gives a principled basis for deriving these relations [14–16, 27]. In addition, the present work also uniquely reckons with the need to establish a complete set of observables, in the First-Law-like component in order to achieve the full power of a Two Laws NEQ theory.

The opportunities and promise of the Two Laws formulation of NEQ: First, CFT is not limited to thermal materials and processes. It can treat forces and flows more generally: not just kinetic cycles or cellular pathways of biochemical or mechanical transformations or of molecules through chemical plants, but also the trafficking of vehicles or goods in supply lines, currents in electrical devices, the flows of evolutionary changes in species or the flows of organisms and resources through ecosystems. It is not limited to heat and work as the main forms of costs and benefits. Our approach can treat other costs and benefits: earnings, profits and taxes, or desired products as benefits vs undesired products as costs.

Second, our approach is not limited by pegging to principles of thermodynamic equilibria, or heat baths, or $k_B T$, or Local Detailed Balance, although it is fully applicable to those situations too. In CFT, Far-From-Equilibrium (FFE) refers to situation that involve either nonlinear force-flow relations and/or not necessarily local equilibrium, whereas in

ST, FFE only refers to the former.

Third, CFT is a complete theory that gives three network forces, one for each type of observable—node populations, traffic on edges, and cycle fluxes. This now opens up a way to advance dynamical modeling in various ways, which we illustrate with several toy examples below. We can understand non-monotonic behaviors, such conflicts or congestion in traffic. We can extend fluctuation-susceptibility relations, such as Maxwell’s and Onsager’s, beyond near-equilibrium [28–30], and beyond inequalities [31, 32], or equalities for specific types of transformation [33, 34], or response relations not yet related to fluctuations [11, 12, 35]. We can model competing tendencies, in the same way that pressure and temperature combine to lead to phase boundaries in equilibrium.

We can devise quantitative criteria for designing networks that optimize desirable behaviors. For example, when CFT is applied to molecular machines powered by ATP hydrolysis, the force conjugated to the net cycle flux in CFT is (half of) the cycle affinity in ST [1], related to the free energy dissipation $(\Delta\mu - w)/(k_B T)$ where $\Delta\mu$ is the free energy difference of ATP hydrolysis and w is the work done by the system per cycle. Under fixed energy source and working conditions, this cycle force is fixed, and CFT provides the remaining coordinate variables to maximize speed, minimize fluctuation, etc. Example 4 below illustrates this.

And, we can get new insights. We show below an extension of Kirchhoff’s Laws of network flows. Kirchhoff’s well-known current and voltage laws of networks describe macro behaviors averaged over many flowing agents. These are derivable from CFT, but CFT also gives an additional relationship based on the edge traffic when fluctuations are not negligible.

DERIVING THE FORCES, CONJUGATE RELATIONS AND LEGENDRE TRANSFORMS IN CFT

Here we show the observable-force coordinates CFT provides, how to (Legendre) transform among these coordinates, and how CFT computes statistical properties and connects fluctuation to susceptibility. Here, we give the procedures and methods; see also [1] for background and derivation.

A. Observable Coordinate, Path Entropy, and the Forces

We first show steps to obtain the observable coordinate and how CFT uses path entropy to define forces. This is in analogue to the microcanonical ensemble in EQ.

Step 1: Define the nodes and edges that constitute the network state space for the process of interest. CFT starts with a given network *state space*, with nodes representing the meso- or micro- states and edges represent Markov transi-

tions. An example is shown in Fig. 1a. We focus on Markov jump processes here, but the framework is generalizable to other Markov or non-Markov process (see [1]). The *phase space* of the various Markov dynamics defined on the same state space are commonly parameterized by transition rates, but CFT, as EQ thermodynamics, seeks a coordinate based on elementary observables. Consider the empirical distribution and fluxes from the trajectory data:

$$\rho_i = \frac{\text{total time spent in node } i}{\text{trajectory length } L}, \quad (3a)$$

$$\rho_{ij} = \frac{\text{total \# of transition } i \mapsto j}{\text{trajectory length } L}. \quad (3b)$$

They converge to probability distribution π_i and flux p_{ij} in the long term, their long-term ratio gives empirical measurement of transition rates $k_{ij} = \lim_{L \rightarrow \infty} \rho_{ij} / \rho_i = p_{ij} / \pi_i$, and they span all first-order, time-additive observables of length- L path $i_{0:L}$ (general costs or benefits) [1, 25]:

$$B[i_{0:L}] = \int_0^L f(i_t) dt + \sum_{t_l} g(i_{t_l^-}, i_{t_l}) \quad (4a)$$

$$= L \sum_i \rho_i f(i) + L \sum_{i \neq j} \rho_{ij} g(i, j) \quad (4b)$$

where $f(i)$ and $g(i, j)$ are production rate of B per unit time dwelling at state i or per transition from i to j , and t_l are the jump times. The set of variables (π_i, p_{ij}) is thus a candidate for the desired observable coordinate, but we must remove its degeneracy due to normalization and steady-state conditions.

Step 2: Choose a node, m (here $m = 1$ in Fig. 1). We intentionally leave it out in the determination of the average distribution π_n , so as to avoid degeneracy in the parameterization. Define a **spanning tree** (a diagram that tiles all nodes without forming a cycle), as illustrated on the left of Fig. 1b. The choices are not unique, and different choices will lead to a different coordinates (linear-algebraic basis) for parameterizing the distributions and fluxes (π_i, p_{ij}) . Users can choose whichever is the most convenient¹.

Step 3: Identify the fundamental cycles by finding cycles formed by adding exactly one edge to the spanning tree [4, 5]. An example is shown in Fig. 1b. Edges outside of the formed cycle are removed, like the edge marked by a red cross on the right of Fig. 1b. These edges that we added to form fundamental cycles define not just the cycles but also the fluxes on them: the average net fluxes J_{ij} on the defining edges is called the *fundamental cycle flux*. For example, in Fig. 1, the first fundamental cycle is 1231, and the fundamental cycle flux is the net flux on edge 12, $J_{\text{cycle},1231} = J_{12} = p_{12} - p_{21}$. Similarly, the second

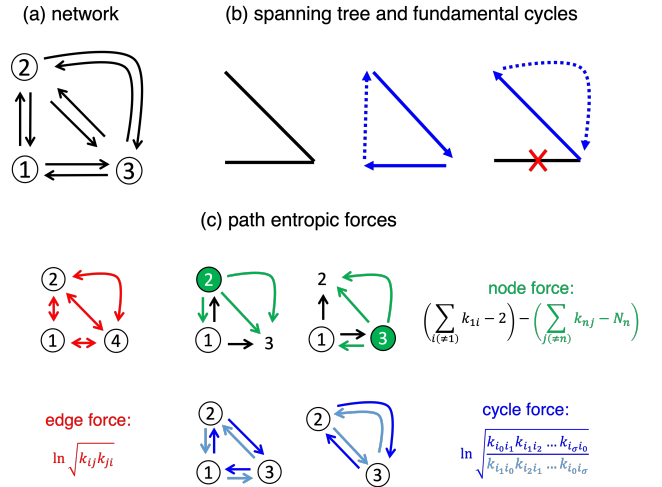


Figure 1. Steps to Find Fundamental Cycles and The Forces for an Example Multi-circular Network: (a) An example network with multiple cycles. (b) A spanning tree of the network, and how to add (dashed) edges to form fundamental cycles. Edges on the spanning tree but not used in forming a cycle is removed, as indicated by the red x. (c) The node, edge, and cycle forces of the example network. k_{ij} is the transition rates from node i to j ; N_n is the number of outgoing edges of node n ; sequence $i_0 i_1 i_2 \dots i_\sigma i_0$ is the sequence defining the cycle, e.g. 1231 and 232 for the two cycles.

fundamental cycle is 232, going through the curved route first then the diagonal route back, and the fundamental cycle flux is $J_{\text{cycle},232} = J_{23}^{\text{urv}}$. The fundamental cycle fluxes superpose all other edge net fluxes on the spanning tree. We have $J_{31} = J_{\text{cycle},1231}$ as cycle 1231 is the only fundamental cycle that passes through it, and $J_{23}^{\text{diag}} = J_{\text{cycle},1231} - J_{\text{cycle},232}$ since both cycles pass through them but the second cycle in opposite direction. With π_n and J_{cycle} specified, the remaining degrees of freedom are the symmetric fluxes on edges, which have been termed traffic $\tau_{ij} = p_{ij} + p_{ji}$ by Maes [36]. Integrating above, we now have a set of distribution and fluxes whose steady-state averages span (π_i, p_{ij}) with no degeneracy [1]. They are $\mathbf{x} = (\pi_{\text{node},n}, \tau_{\text{edge},ij}, J_{\text{cycle},c})$ where $n = 2, 3$ goes through all nodes except node $m = 1$, ij goes through all edges, and $c = 1231, 232$ goes through all fundamental cycles. This variable set \mathbf{x} is CFT's observable coordinate for NEQ, similar to the (U, V, N) in EQ.

Step 4: Compute the path entropy and the forces. As the thermodynamic entropy in EQ is a function of the observables (U, V, N) , the entropy function of NEQ in CFT is a function of the dynamic observables $\mathbf{x} = (\pi_{\text{node},n}, \tau_{\text{edge},ij}, J_{\text{cycle},c})$. CFT's entropy $\mathfrak{s}_{\text{path}}(\mathbf{x})$ is the path entropy rate relative to a reference process, here chosen to be the one with unit rates $u_{ij} = 1$ [1]. Denoting $P_k(i_{0:L})$ as the probability of path $i_{0:L}$

¹ CFT tackles the system's dynamical response to varying various parameter knobs. From the analysis standpoint, the most convenient coordinate is the one with the smallest number of forces being controlled by those knobs.

in the Markov process with transition rates k_{ij} , we have [1]

$$\mathfrak{s}_{\text{path}}(\mathbf{x}) = \lim_{L \rightarrow \infty} \frac{1}{L} \left[- \sum_{i_{0:L}} P_k(i_{0:L}) \ln \frac{P_k(i_{0:L})}{P_u(i_{0:L})} \right] \quad (5a)$$

$$= \sum_{i \neq j} p_{ij}(\mathbf{x}) - \pi_i(\mathbf{x}) - p_{ij}(\mathbf{x}) \ln \frac{p_{ij}(\mathbf{x})}{\pi_i(\mathbf{x})} \quad (5b)$$

where $\pi_i(\mathbf{x})$ and $p_{ij}(\mathbf{x})$ are spanned by $\mathbf{x} = (\pi_{\text{node},n}, \tau_{\text{edge},ij}, J_{\text{cycle},c})$ based on Steps 2 and 3. Forces conjugated to the observables \mathbf{x} are the derivatives of the path entropy (rate):

$$\mathfrak{F} = - \frac{\partial \mathfrak{s}_{\text{path}}}{\partial \mathbf{x}}. \quad (6)$$

This is in analogue to defining $(1/T, P/T, -\mu/T)$ from EQ entropy derivative in microcanonical ensemble. CFT can further express these forces of NEQ meaningfully with the transition rates locally defined on nodes, edge, and cycles, as shown in Fig. 1c (See [1] for derivations). This allows dynamical interpretations of the forces: they represent the relative tendency to stay on a node, the affinity for a back-and-forth motion on an edge, and the relative affinity to complete a forward cycle over the backward.

Defining forces as path entropic force in Eq. (6) has two immediate implications. First, path entropy $\mathfrak{s}_{\text{path}}(\mathbf{x})$ is a strictly-concave function of the phase space under the \mathbf{x} coordinate:

$$\frac{\partial \mathfrak{F}}{\partial x} = - \frac{\partial^2 \mathfrak{s}_{\text{path}}}{\partial x^2} > 0 \quad (7)$$

where x can be any of $(\pi_{\text{node},n}, \tau_{\text{edge},ij}, J_{\text{cycle},c})$ and \mathfrak{F} is its conjugated force. This is the first manifestation of conjugacy—the level of force increases monotonically in the transformation where we tune its conjugated observable and fix all others. See [27] for how this curvature of $(-\mathfrak{s}_{\text{path}})$ represents “the fluctuation of forces”. Second, Eq. (6) expresses forces as functions of observables $\mathfrak{F}(\mathbf{x})$, converting the force coordinate to the observable coordinate. Below, we show the inverse—how to get $\mathbf{x}(\mathfrak{F})$.

B. Force Coordinate and Statistical Properties Computation

CFT uses the Caliber (rate) to convert from the observable coordinate \mathbf{x} to the force coordinate \mathfrak{F} . It is the logarithmic rate of the partition function for dynamics, parameterized by the forces \mathfrak{F} :

$$\mathfrak{c}(\mathfrak{F}) = \lim_{L \rightarrow \infty} \frac{1}{L} \ln \sum_{i_{0:L}} P_u(i_{0:L}) e^{\mathfrak{F} \cdot \mathbf{X}(i_{0:L})} \quad (8)$$

where P_u is the path probability of the unit-rate process—the *doldrum process* at the origin $\mathfrak{F} = \mathbf{0}$ of the force coordinate—and $\mathbf{X}(i_{0:L})$ is a vector of counting observables whose long-term rates are \mathbf{x} , $\lim_{L \rightarrow \infty} \mathbf{X}(i_{0:L})/L = \mathbf{x}$. This counting observable vector has three groups of components $\mathbf{X} =$

$(X_{\text{node},n}, X_{\text{edge},ij}, X_{\text{cycle},c})$. With δ_{ij} denoting the Kronecker delta function, the first group is the total dwell time of node:

$$X_{\text{node},n} = \int_0^L \delta_{i_t,n} dt. \quad (9)$$

It has long-term rate $\pi_{\text{node},n}$ and gives the total dwell time in node n ; The second group is the total traffic of edge ij (total counts of edge taken, either way):

$$X_{\text{edge},ij} = \sum_{\text{jump } l} \delta_{i_t^-,i} \delta_{i_t^+,j} + \delta_{i_t^-,j} \delta_{i_t^+,i} \quad (10)$$

where i_t^\pm represents the state immediately before/after the l -th jump. It has long-term rate $\tau_{\text{edge},ij}$ and gives the total counts across the ij edge, regardless of which direction; The last group is net counts for the edge ab that defines the fundamental cycle c :

$$X_{\text{cycle},c} = \sum_{\text{jump } l} \delta_{i_t^-,a} \delta_{i_t^+,b} - \delta_{i_t^-,b} \delta_{i_t^+,a}. \quad (11)$$

It has components with long-term rate $J_{\text{cycle},c}$.

The Caliber (rate) $\mathfrak{c}(\mathfrak{F})$ is linearly related to the scaled cumulant generating function of \mathbf{X} in the process parameterized by the forces \mathfrak{F} : $G_{\mathfrak{F}}(\theta) = \mathfrak{c}(\mathfrak{F} + \theta) - \mathfrak{c}(\mathfrak{F})$ [1]. Its first derivatives give the average rates \mathbf{x} of \mathbf{X} :

$$\mathbf{x} = \frac{\partial \mathfrak{c}}{\partial \mathfrak{F}}; \quad (12)$$

and the second derivatives give the long-term, scaled (co)variances of \mathbf{X} :

$$\frac{\partial^2 \mathfrak{c}}{\partial \mathfrak{F}^2}(\mathfrak{F}) = \lim_{L \rightarrow \infty} \frac{\text{Var}[X]}{L} > 0; \quad (13a)$$

$$\frac{\partial^2 \mathfrak{c}}{\partial \mathfrak{F} \partial \mathfrak{F}'}(\mathfrak{F}) = \lim_{L \rightarrow \infty} \frac{\text{CoV}[X, X']}{L}. \quad (13b)$$

where X, X' can be any two of $(X_{\text{node},n}, X_{\text{edge},ij}, X_{\text{cycle},c})$ and $\mathfrak{F}, \mathfrak{F}'$ are their conjugated forces.

We get four immediate implications. First, Eq. (12) converts the observable coordinate \mathbf{x} to the force coordinate \mathfrak{F} , which is the desired inverse of Eq. (6); Second, Eq. (12) and Eq. (13) together shows how fluctuations relate to the response of \mathbf{x} to forces—the *fluctuation-susceptibility equalities* of NEQ. Third, Eq. (12) and Eq. (13a) combined gives $\partial x / \partial \mathfrak{F} > 0$ where \mathfrak{F} is the conjugated force of x , the second manifestation of conjugacy. Last but not least, Eq. (12) and Eq. (13b) gives $\partial x / \partial \mathfrak{F}' = \partial x' / \partial \mathfrak{F}$, which is the NEQ generalization of Maxwell relation in EQ and Onsager reciprocity in near EQ. We show how to further express $\mathfrak{c}(\mathfrak{F})$ and its derivatives in terms of the transition rates k_{ij} , with Figure 1 as the guiding example.

Step 1: Reference the *doldrum state* conditions. Now express the Markov transition matrix of the *doldrum state* (for

the example in Figure 1):

$$\mathbf{M} = \begin{bmatrix} -2 & 1 & 1 \\ 1 & -3 & 1+1 \\ 1 & 1+1 & -3 \end{bmatrix}. \quad (14)$$

This is essentially a connectivity matrix with diagonal components showing the out-degree of each the nodes (the negative transpose of Laplacian matrix in graph theory). Then, we **write down** a matrix $\tilde{\mathbf{M}}$ of forces based on the observables (called **the tilted matrix** in large deviation theory [25, 27, 37, 38]). For simplicity, let's drop the annotation of node/edge/cycle and denote $\tilde{\mathfrak{F}}_{23}^{\text{diag}} = \tilde{\mathfrak{F}}_{23}$, $\tilde{\mathfrak{F}}_{23}^{\text{curv}} = \tilde{\mathfrak{F}}'_{23}$, $\tilde{\mathfrak{F}}_{1231} = \tilde{\mathfrak{F}}_{\Delta}$, and $\tilde{\mathfrak{F}}_{232} = \tilde{\mathfrak{F}}_{\nabla}$. The tilted matrix is then

$$\tilde{\mathbf{M}} = \begin{bmatrix} -2 & e^{\tilde{\mathfrak{F}}_{12} + \tilde{\mathfrak{F}}_{\Delta}} & e^{\tilde{\mathfrak{F}}_{13}} \\ e^{\tilde{\mathfrak{F}}_{12} - \tilde{\mathfrak{F}}_{\Delta}} & \tilde{\mathfrak{F}}_2 - 3 & e^{\tilde{\mathfrak{F}}_{23}} + e^{\tilde{\mathfrak{F}}'_{23} + \tilde{\mathfrak{F}}_{\nabla}} \\ e^{\tilde{\mathfrak{F}}_{13}} & e^{\tilde{\mathfrak{F}}_{23}} + e^{\tilde{\mathfrak{F}}'_{23} - \tilde{\mathfrak{F}}_{\nabla}} & \tilde{\mathfrak{F}}_3 - 3 \end{bmatrix}.$$

We put $\tilde{\mathfrak{F}}_n$ on $\tilde{\mathbf{M}}_{nn}$ for $n = 2, 3$ since we measure their π_n ; We put $\tilde{\mathfrak{F}}_{ij}$ symmetrically on both $\tilde{\mathbf{M}}_{ij}$ and $\tilde{\mathbf{M}}_{ji}$ because the traffic on ij measures the sum of fluxes both ways; We put $\tilde{\mathfrak{F}}_{\Delta}$ positively on $\tilde{\mathbf{M}}_{12}$ and negatively on $\tilde{\mathbf{M}}_{21}$ because the fundamental cycle flux of cycle 1231 is defined on the net flux on the transition $1 \mapsto 2$. The same goes for how the other cycle force $\tilde{\mathfrak{F}}_{\nabla}$ is introduced on the curved-edge components of $\tilde{\mathbf{M}}_{23}$ and $\tilde{\mathbf{M}}_{32}$.

Step 2: Use the Caliber $c(\mathfrak{F})$ to compute statistical properties. The caliber defined in Eq. (8) is the largest eigenvalue of the tilted matrix $\tilde{\mathbf{M}}$ [1]. Similar to steps in Koza [39] or in Barato and Seifert [38], the statistical cumulants (average, variance, etc) of \mathbf{X} can be computed iteratively. The caliber satisfies the characteristic equation:

$$\det(\tilde{\mathbf{M}} - c \mathbf{I}) = 0 \quad (15)$$

where \mathbf{I} is the identity matrix. Since the determinant on the left is a polynomial of c , taking the first derivative with respect to a given force \mathfrak{F} can give us the first derivative $\partial c / \partial \mathfrak{F}$ in terms of c and all forces \mathfrak{F} . Taking a second derivative will relate the second derivative, the Caliber c , and the first derivatives. Higher order derivatives can then be evaluated iteratively.

Step 3: Expressing Caliber and Forces in terms of rates. Based on Max Cal and LDT [1], the transition rate matrix \mathbf{K} is a similarity transform of the tilted matrix subtracted by $c \mathbf{I}$:

$$\mathbf{K} = \mathbf{R}^{-1}(\tilde{\mathbf{M}} - c \mathbf{I})\mathbf{R} \quad (16)$$

where $\mathbf{R} = \text{diag}(r_1, r_2, \dots, r_N)$ is a diagonal matrix with \mathbf{r} being the (right) eigenvector corresponding the the largest eigenvalue of the tilted matrix $\tilde{\mathbf{M}}$. In components, they are $\mathbf{K} = [k_{ij}] =$

$$\begin{bmatrix} -2 - c & \frac{r_2}{r_1} e^{\tilde{\mathfrak{F}}_{12} + \tilde{\mathfrak{F}}_{\Delta}} & \frac{r_3}{r_1} e^{\tilde{\mathfrak{F}}_{13}} \\ \frac{r_1}{r_2} e^{\tilde{\mathfrak{F}}_{12} - \tilde{\mathfrak{F}}_{\Delta}} & \tilde{\mathfrak{F}}_2 - 3 - c & \frac{r_3}{r_2} (e^{\tilde{\mathfrak{F}}_{23}} + e^{\tilde{\mathfrak{F}}'_{23} + \tilde{\mathfrak{F}}_{\nabla}}) \\ \frac{r_1}{r_3} e^{\tilde{\mathfrak{F}}_{13}} & \frac{r_2}{r_3} (e^{\tilde{\mathfrak{F}}_{23}} + e^{\tilde{\mathfrak{F}}'_{23} - \tilde{\mathfrak{F}}_{\nabla}}) & \tilde{\mathfrak{F}}_3 - 3 - c \end{bmatrix}.$$

This gives expressions of forces in terms of the posterior transition rates k_{ij} , as shown in Fig.1c, and that the Caliber can be related to the (posterior) escape rate of the reference node $m = 1$ (plus the number of edges attached to it):

$$c = k_{12} + k_{13} - 2. \quad (17)$$

See [1] for derivations. With this, one can circumvent the largest eigenvalue calculation and express all statistical cumulants in terms of the transition rates. This gives analytical solutions of the statistical cumulants of the fundamental counting observables \mathbf{X} —consistent to past approaches such as Hill's diagram method [4, 5, 38]—and more importantly the interpretations of the forces. What's new here are *not* these analytical expressions *but* that these computational methods come with the full thermodynamic-like conjugate structure between observables and forces for NEQ as well as between path entropy and caliber, which we now summarize.

C. Legendre Transform and Mixed Coordinates

Coordinate conversion summarized by Legendre Transform. We have shown how to use the path entropy $s_{\text{path}}(\mathbf{x})$ and the caliber $c(\mathfrak{F})$ to convert between the observable coordinate \mathbf{x} and the force coordinate \mathfrak{F} . As in EQ, the dual coordinate conversion is summarized by Legendre transform

$$c(\mathfrak{F}) = \mathfrak{F} \cdot \mathbf{x} + s_{\text{path}}(\mathbf{x}), \quad (18)$$

which is evaluated in either \mathbf{x} or \mathfrak{F} . To recap, on the one hand, taking derivative of Eq. (18) under the \mathbf{x} coordinate gives

$$\frac{\partial c}{\partial \mathfrak{F}} \cdot \frac{\partial \mathfrak{F}}{\partial \mathbf{x}} = \frac{\partial \mathfrak{F}}{\partial \mathbf{x}} \cdot \mathbf{x} + \mathfrak{F} + \frac{\partial s_{\text{path}}}{\partial \mathbf{x}} \quad (19)$$

With concave s_{path} and forces defined as $\mathfrak{F} = -\partial s_{\text{path}} / \partial \mathbf{x}$, the matrix $\partial \mathfrak{F} / \partial \mathbf{x}$ is invertible, and the equation gives $\mathbf{x} = \partial c / \partial \mathfrak{F}$. On the other hand, under the \mathfrak{F} coordinate, we get

$$\frac{\partial c}{\partial \mathfrak{F}} = \mathbf{x} + \mathfrak{F} \cdot \frac{\partial \mathbf{x}}{\partial \mathfrak{F}} + \frac{\partial s_{\text{path}}}{\partial \mathbf{x}} \cdot \frac{\partial \mathbf{x}}{\partial \mathfrak{F}}. \quad (20)$$

With convex c (linear to generating function) and $\mathbf{x} = \partial c / \partial \mathfrak{F}$, the matrix $\partial \mathbf{x} / \partial \mathfrak{F}$ is invertible, and one gets back $\mathfrak{F} = -\partial s_{\text{path}} / \partial \mathbf{x}$.

Computing the covariance matrix by inverting the Hessian of path entropy. The negative of path entropy ($-s_{\text{path}}$) and the caliber c are convex conjugate to each other [40] with reciprocal curvatures [1, 27]. The Hessian matrix of them are the two matrices above— $\partial \mathfrak{F} / \partial \mathbf{x}$ for ($-s_{\text{path}}$) and $\partial \mathbf{x} / \partial \mathfrak{F}$ for c —and are inverse matrices to each other. This has an uncertain principle interpretation [27]. Since s_{path} is much easier to evaluate than c , its Hessian is also easier to compute. We can thus compute the Hessian of c —i.e. the covariance matrix of \mathbf{X} —by inverting the Hessian of ($-s_{\text{path}}$). This is numerically easier than the direct computation from taking derivatives of the characteristic equation of c under the force coordinate and can also reveal new relations between the fluctuation of \mathbf{X} with their averages \mathbf{x} . We will illustrate

these with examples later. Note that the inverse of covariance matrix—i.e. the Hessian of $(-\mathfrak{s}_{\text{path}})$ —has been called the “precision matrix” in statistics.

Fluctuation-Susceptibility Equalities in mixed Coordinates: The conversion between \mathbf{x} and \mathfrak{F} is through a full Legendre transform that swap all variables with their conjugates. As in EQ, we can obtain a zoo of mixed coordinates through partial Legendre transform. These new coordinates are useful in characterizing various effects of parameter tunings and in solving optimization problem constrained on mixes of observables and forces, illustrated with more examples later. Here, we present the abstract, general case on how to get those mixed coordinates and to derive Maxwell-Onsager symmetry as well as fluctuation-susceptibility equalities in these coordinates.

Consider a generic mixed coordinate $z = (\mathfrak{F}_1, \mathbf{x}_2)$ with N_1 number of force variables \mathfrak{F}_1 and N_2 number of observable variables \mathbf{x}_2 . With $\phi(z)$ as the “thermodynamic-like” potential in z , Legendre transform gives

$$-\phi = \mathfrak{F}_1 \cdot \mathbf{x}_1 + \mathfrak{s}_{\text{path}}; \quad (21a)$$

$$\phi = \mathfrak{F}_2 \cdot \mathbf{x}_2 - \mathbf{c}. \quad (21b)$$

Under the mixed coordinate z , we can compute $\mathbf{x}_1(z)$ and $\mathfrak{F}_2(z)$ by the partial derivatives of $\phi(z)$:

$$\mathbf{x}_1 = -\frac{\partial \phi}{\partial \mathfrak{F}_1}; \quad \mathfrak{F}_2 = \frac{\partial \phi}{\partial \mathbf{x}_2} \quad (22)$$

where Maxwell-Onsager symmetry immediately follows from taking a second derivative.

To relate the susceptibility of \mathbf{x}_1 or \mathfrak{F}_2 to the fluctuation of the elementary counting observables \mathbf{X} , we consider the two implicit equations associated with the Caliber:

$$\mathbf{x}_1(z) = \frac{\partial \mathbf{c}}{\partial \mathfrak{F}_1}[\mathfrak{F}_1, \mathfrak{F}_2(z)] \quad (23a)$$

$$\mathbf{x}_2 = \frac{\partial \mathbf{c}}{\partial \mathfrak{F}_2}[\mathfrak{F}_1, \mathfrak{F}_2(z)]. \quad (23b)$$

For later notation simplicity, let us introduce four shorthands: $\mathbf{C}_{11} = \partial^2 \mathbf{c} / \partial \mathfrak{F}_1^2$ is a N_1 -by- N_1 square covariance matrix of the components of \mathbf{X}_1 ; $\mathbf{C}_{22} = \partial^2 \mathbf{c} / \partial \mathfrak{F}_2^2$ is a N_2 -by- N_2 square covariance matrix of the components of \mathbf{X}_2 ; $\mathbf{C}_{12} = \partial^2 \mathbf{c} / \partial \mathfrak{F}_1 \partial \mathfrak{F}_2$ is a N_1 -by- N_2 matrix with covariance terms between \mathbf{X}_1 and \mathbf{X}_2 ; And, $\mathbf{C}_{21} = \mathbf{C}_{12}^T$ is a N_2 -by- N_1 matrix, the transpose of \mathbf{C}_{12} . Then, by taking partial derivatives with respect to \mathbf{x}_2 and \mathfrak{F}_1 of Eqs. (23), we get the desired fluctuation-susceptibility equalities [41]:

$$\frac{\partial \mathbf{x}_1}{\partial \mathfrak{F}_1}(z) = \mathbf{C}_{11} - \mathbf{C}_{12} \mathbf{C}_{22}^{-1} \mathbf{C}_{21} \quad (24a)$$

$$\frac{\partial \mathbf{x}_1}{\partial \mathbf{x}_2}(z) = \mathbf{C}_{12} \mathbf{C}_{22}^{-1} \quad (24b)$$

$$\frac{\partial \mathfrak{F}_2}{\partial \mathfrak{F}_1}(z) = -\mathbf{C}_{22}^{-1} \mathbf{C}_{21} \quad (24c)$$

$$\frac{\partial \mathfrak{F}_2}{\partial \mathbf{x}_2}(z) = \mathbf{C}_{22}^{-1}. \quad (24d)$$

These are not new math for those familiar with Legendre transform, but these coordinates and fluctuation-susceptibility relations for NEQ, as far as our knowledge, are new.

ILLUSTRATING THE THEORY WITH SIMPLE APPLICATIONS

We present five examples here. Our first example illustrates CFT’s thermodynamic-like *conjugacy* in the simplest two-dimensional dynamics of a chemical receptor; The second example illustrates the *necessity of the full set* of forces—not just the time irreversible one in ST—in a simple NEQ model of non-thermal unicircular truck delivery dynamics; The third example shows how *mixed coordinates* in CFT help analyze a toy non-thermal traffic congestion problem; Our fourth example shows how CFT’s coordinates help us analyze *constrained optimization* for a toy molecular motor model; Our last example discusses stochastic particle transport in multi-cycle circuits/channels and how CFT helps the *generalization of Ohm’s law and Kirchhoff’s laws*.

Example 1. Two-state Chemical Receptor illustrates Conjugacy and Fluctuation-Susceptibility Equalities.

We follow [42] to consider a two-state single receptor Markov model. Suppose state 1 is the unbound state of the receptor and 2 is the bound state. The dynamics is two-dimensional and can be specified by the two Markov transition rates $k_{12} = \tau_b^{-1} c / c_0$ and $k_{21} = \tau_b^{-1}$ where τ_b is the average bound time, c is the chemical concentration and c_0 is the concentration where $k_{12} = k_{21}$:

$$\text{unbound} \xrightleftharpoons[k_{21}]{k_{12}} \text{bound}$$

Suppose the long-term time fraction in the unbound state 1 is π_1 and the traffic of binding and unbinding is $\tau = \pi_1 k_{12} + \pi_2 k_{21}$. These two observables $\mathbf{x} = (\pi_1, \tau)$ can serve as CFT’s observable coordinate. Rates can be expressed by observables: $k_{12} = \tau / (2\pi_1)$ and $k_{21} = \tau / [2(1 - \pi_1)]$, and from which $\pi_1 = k_{21} / (k_{12} + k_{21})$ and $\tau = 2k_{12}k_{21} / (k_{12} + k_{21})$. We have chosen to leave out the distribution measurement of the bound state ($m = 2$ based on notation above). There is no cycle flux in this example because a two-node-one-edge system must obey detailed balance, but the formalism applies to NEQ, as we’ll show in other examples.

Path Entropy and Forces: Using Eq. (5), the path entropy of this example is

$$\mathfrak{s}_{\text{path}}(\mathbf{x}) = \tau - 1 - \frac{\tau}{2} \ln \frac{\tau^2}{4\pi_1(1 - \pi_1)} \quad (25)$$

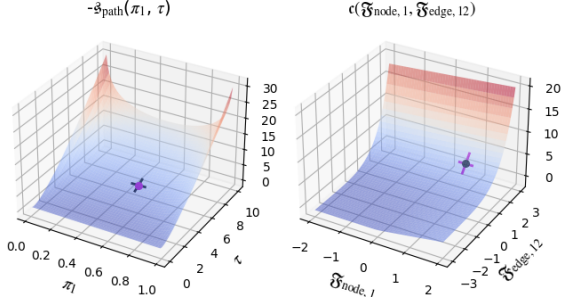


Figure 2. **Conjugacy between Path Entropy and Caliber.** The two figures demonstrate the phase space of the two-state chemical receptor in observable coordinate and in force coordinate, and the “thermodynamic-like” potentials defined on them—path entropy s_{path} and the Caliber c . The negative path entropy $-s_{\text{path}}(\mathbf{x})$ is given by Eq. (25) and the conjugated Caliber $c(\mathfrak{F})$ is given by Eq. (29). The Legendre transform between $(-s_{\text{path}})$ and c is a point-slope conversion. Purple dot on the left is an example process specified by the observables $(\pi_1, \tau) = (0.55, 5)$, which are the slopes in the purple cross in the plot on the right. The slopes of the black cross on the left are $(\mathfrak{F}_1, \mathfrak{F}_{12}) \approx (1.01, 1.61)$ given by Eq. (26), which are the coordinate for the black dot on the right. The two cross dots represent the same process in two coordinate spaces.

The forces in terms of the observables are then

$$\mathfrak{F}_1 = -\frac{\partial s_{\text{path}}}{\partial \pi_1} = \frac{\tau}{2(1-\pi_1)} - \frac{\tau}{2\pi_1} = k_{21} - k_{12} \quad (26a)$$

$$\mathfrak{F}_{12} = -\frac{\partial s_{\text{path}}}{\partial \tau} = \ln \frac{\tau}{4\sqrt{\pi_1(1-\pi_1)}} = \frac{1}{2} \ln k_{12}k_{21}. \quad (26b)$$

In this simple example, the rates under the force coordinate can be solve directly from the two equations above:

$$k_{12}(\mathfrak{F}) = \frac{1}{2} \left(\sqrt{\mathfrak{F}_1^2 + 4e^{2\mathfrak{F}_{12}}} - \mathfrak{F}_1 \right) \quad (27a)$$

$$k_{21}(\mathfrak{F}) = \frac{1}{2} \left(\sqrt{\mathfrak{F}_1^2 + 4e^{2\mathfrak{F}_{12}}} + \mathfrak{F}_1 \right). \quad (27b)$$

Nevertheless, we demonstrate below the systematic method from tilted matrix and eigenvalue.

Caliber and Legendre Transform: The tilted matrix in this example is simply

$$\tilde{\mathbf{M}} = \begin{bmatrix} \mathfrak{F}_1 - 1 & e^{\mathfrak{F}_{12}} \\ e^{\mathfrak{F}_{12}} & -1 \end{bmatrix}. \quad (28)$$

The largest eigenvalue—i.e. the caliber $c(\mathfrak{F})$ —takes the expected form (c.f. Eq. (17)) of

$$c = k_{21}(\mathfrak{F}) - 1. \quad (29)$$

Its derivatives, as expected, give back \mathbf{x} :

$$\frac{\partial c}{\partial \mathfrak{F}_1} = \frac{\mathfrak{F}_1}{2\sqrt{\mathfrak{F}_1^2 + 4e^{2\mathfrak{F}_{12}}}} + \frac{1}{2} = \frac{k_{21}}{k_{12} + k_{21}} = \pi_1 \quad (30a)$$

$$\frac{\partial c}{\partial \mathfrak{F}_{12}} = \frac{2e^{2\mathfrak{F}_{12}}}{\sqrt{\mathfrak{F}_1^2 + 4e^{2\mathfrak{F}_{12}}}} = \frac{2k_{12}k_{21}}{k_{12} + k_{21}} = \tau. \quad (30b)$$

Figure 2 depicts the two “thermodynamic potentials” ($-s_{\text{path}}(\mathbf{x})$) and $c(\mathfrak{F})$ in the observable and force coordinates, convex conjugated to each other and related by Legendre transform:

$$c = \mathfrak{F}_1 \pi_1 + \mathfrak{F}_{12} \tau + s_{\text{path}}. \quad (31)$$

Fluctuation and Susceptibilities: The susceptibility of $\mathbf{x} = (\pi_1, \tau)$ to forces $\mathfrak{F} = (\mathfrak{F}_1, \mathfrak{F}_{12})$ can be computed straightforwardly by taking another force derivatives of Eqs. (30), which we don’t carry out here. Instead, we show how to find relations between fluctuation and averages, using the inverse relation between the Hessian of caliber and the Hessian of negative path entropy. The Hessian of negative path entropy is

$$\mathbf{H}_{(-s)} = \begin{bmatrix} \frac{\tau[\pi^2 + (1-\pi)^2]}{2\pi^2(1-\pi)^2} & \frac{\pi - \frac{1}{2}}{\pi(1-\pi)} \\ \frac{\pi - \frac{1}{2}}{\pi(1-\pi)} & \frac{1}{\tau} \end{bmatrix}, \quad (32)$$

and its inverse is $\mathbf{H}_c = \mathbf{H}_{(-s)}^{-1}$

$$= \begin{bmatrix} \frac{4}{\tau} \pi^2 (1-\pi)^2 & (2-4\pi)\pi(1-\pi) \\ (2-4\pi)\pi(1-\pi) & 2\tau[\pi^2 + (1-\pi)^2] \end{bmatrix}. \quad (33)$$

Denoting $X_{\text{node},1}$ as the total time in the unbound state for a length L trajectory and $X_{\text{edge},12}$ as the total counts of binding and unbinding events, their average rates are π_1 and τ , and \mathbf{H}_c gives their (scaled) long-term fluctuation:

$$\sigma_\pi^2 = \lim_{L \rightarrow \infty} \frac{\text{Var}[X_{\text{node},1}]}{L} = \frac{4}{\tau} \pi^2 (1-\pi)^2 \quad (34a)$$

$$\sigma_\tau^2 = \lim_{L \rightarrow \infty} \frac{\text{Var}[X_{\text{edge},12}]}{L} = 2\tau[\pi^2 + (1-\pi)^2]. \quad (34b)$$

The off-diagonal terms are their scaled covariance.

Following [42–44], we compute the infinitesimal changes in $\mathbf{x} = (\pi_1, \tau)$ due to the tuning of chemical concentration dc . In CFT, we span the changes by the infinitesimal force perturbations $d\mathfrak{F}$ due to dc and use the covariance matrix as the susceptibility matrix:

$$d\mathbf{x} = \mathbf{H}_c d\mathfrak{F}. \quad (35)$$

The $d\mathfrak{F}$ can be evaluated by partial derivatives of the rate-expression of forces in Eq. (26) with respect to c . After simplification [41], we get:

$$c \frac{\partial \pi_1}{\partial c} = -\pi(1-\pi) \quad (36a)$$

$$c \frac{\partial \tau}{\partial c} = \pi\tau. \quad (36b)$$

And, the fluctuation-response ratios—the so-called “inference times” considered in [42]—take the following simple forms in terms of the observables:

$$\frac{\sigma_\pi^2}{(c \frac{\partial \pi_1}{\partial c})^2} = \frac{4}{\tau} \quad (37a)$$

$$\frac{\sigma_\tau^2}{(c \frac{\partial \tau}{\partial c})^2} = \frac{2}{\tau} \left[1 + \left(\frac{1-\pi}{\pi} \right)^2 \right]. \quad (37b)$$

A well-known result can be clearly seen under this parameterization with the average dynamic observables: when the chemical concentration is low $c \ll c_0$, the receptor spent most of its time in the unbound state $\pi \rightarrow 1$. Then, the ratio for the traffic is half of that for the distribution, consistent to past results [42, 44]. Eq. (37b) further shows that (a) it is the minimum under fixed traffic and (b) increasing traffic reduce both ratios.

We introduce this simplest two-dimensional example to illustrate CFT's methods, show visualizations of the two conjugated potentials, and simply demonstrate consistency with past results.

Example 2. In some cases, forces anti-correlate with flows.

Because networks have three component forces, situations can arise where one component force has the opposite sign of changes from its corresponding flow. First, let's consider a switch of variables. For a unicyclic process, the cycle force can be expressed under the observable coordinate \mathbf{x} as:

$$\mathfrak{F}_{\text{cycle}} = \frac{1}{2} \ln \prod_z \frac{\tau_z + J_{\text{cycle}}}{\tau_z - J_{\text{cycle}}} \quad (38)$$

where z goes over edges on the cycle. As have been proven in Eq. (7), increasing cycle force is generally expected to increase the net flux but is only guaranteed when traffic terms are fixed. When traffic terms vary as well, the conjugated cycle force and flux can have opposite trends.

Here, we illustrate such ‘‘conflict’’ where the cycle force opposes the net flux, in a non-thermal stochastic truck dynamics example. One truck driver, Alice, follows the simple unicyclic delivery network in Fig. 3. Assume Alice has a delivery and warehouse-return rate of f and backtrack rate of ϵf . Another truck driver, Bob, has forward rate f' and backward rate $\epsilon' f'$. Suppose that Bob has a higher error rate $\epsilon' > \epsilon$. We explore the consequences of Bob's different potential values f' .

Evaluating Average Fluxes and Forces. Each cargo's dynamics with Alice and Bob together as a team can be described by a two-node-two-edge Markov model shown in Fig. 3(a). The dynamics is four dimensional, and we can use the cargo distribution at the warehouse π , the edge traffic of delivery and return τ_d, τ_r , and the cycle flux J_{cycle} as the observable coordinate $\mathbf{x} = (\pi, \tau_d, \tau_r, J_{\text{cycle}})$. The conjugated forces are then $\mathfrak{F} = (\mathfrak{F}_{\text{node}}, \mathfrak{F}_d, \mathfrak{F}_r, \mathfrak{F}_{\text{cycle}})$. For presentation simplicity, we assume symmetry in delivery and return, which leads to uniform $\pi = 1/2$ and $\tau_d = \tau_r = \tau_{\text{edge}}$. We can then evaluate

$$\tau_{\text{edge}} = \frac{f + \epsilon f}{2} + \frac{f' + \epsilon' f'}{2} \quad (39a)$$

$$J_{\text{cycle}} = \frac{f - \epsilon f}{2} + \frac{f' - \epsilon' f'}{2} \quad (39b)$$

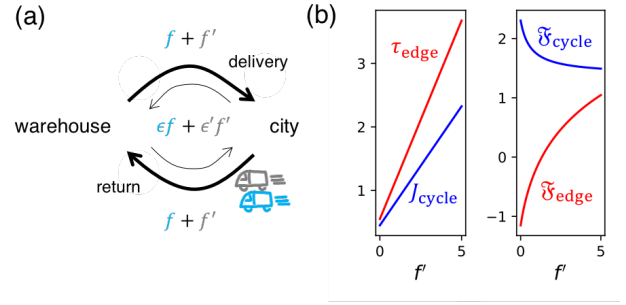


Figure 3. **A truck example shows conjugated flux and force can have opposite trends due to other varying forces.** (a) shows the effective transition rates of two symmetric truck drivers, the blue one (Alice) with forward jump rate $f = 1$ and backward jump rate $\epsilon f = 0.1$ and the gray one (Bob) with undetermined forward jump rate f' and a fixed backward rate $\epsilon' f' = 0.25 f'$. (b) shows the opposite trends of cycle force and cycle flux in blue, which is due to the increasing traffic and edge force.

The node force $\mathfrak{F}_{\text{node}}$ is zero due to symmetry, and the other forces are

$$\mathfrak{F}_{\text{edge}} = \frac{1}{2} \ln(f + f')(\epsilon f + \epsilon' f') \quad (40a)$$

$$\mathfrak{F}_{\text{cycle}} = \ln \frac{f + f'}{\epsilon f + \epsilon' f'}. \quad (40b)$$

If Bob's f' increases, the cycle force decreases while the net flux increases as shown in Fig. 3(b). The opposite trends between the conjugated pair is because of the increasing traffic τ and edge force $\mathfrak{F}_{\text{edge}}$, as explained below.

Decomposing Responses with Forces. Of interest here are the responses of net flux due to the tuning of a system parameter f' . Under the force coordinate, the change of the flux J_{cycle} is decomposed into contributions from the changes in different forces:

$$\frac{dJ_{\text{cycle}}}{df'} = \sum_{\mathfrak{F} \in \mathfrak{F}} \frac{\partial J_{\text{cycle}}}{\partial \mathfrak{F}} \frac{\partial \mathfrak{F}}{\partial f'} \quad (41)$$

where \mathfrak{F} runs through $(\mathfrak{F}_{\text{node}}, \mathfrak{F}_{\text{delivery}}, \mathfrak{F}_{\text{return}}, \mathfrak{F}_{\text{cycle}})$. Here, due to the assumed symmetry, we get the following simplified form:

$$\frac{dJ_{\text{cycle}}}{df'} = 2 \underbrace{\frac{\partial J_{\text{cycle}}}{\partial \mathfrak{F}_{\text{edge}}}}_{>0} \underbrace{\frac{\partial \mathfrak{F}_{\text{edge}}}{\partial f'}}_{>0} + \underbrace{\frac{\partial J_{\text{cycle}}}{\partial \mathfrak{F}_{\text{cycle}}}}_{>0} \underbrace{\frac{\partial \mathfrak{F}_{\text{cycle}}}{\partial f'}}_{<0} \quad (42)$$

This shows that the opposite trends between cycle flux J_{cycle} and cycle force $\mathfrak{F}_{\text{cycle}}$ is because the positive effect from increasing edge forces overwhelms the effect from decreasing cycle force.

Here is how the four terms are computed. The derivatives of the forces with respect to f' can be computed directly from Eq. (40), showing that $\partial \mathfrak{F}_{\text{edge}} / \partial f' > 0$ and $\partial \mathfrak{F}_{\text{cycle}} / \partial f' < 0$ [41]. The coefficient $\partial J_{\text{cycle}} / \partial \mathfrak{F}_{\text{cycle}} > 0$ is the asymptotic

variance of cycle flux and is thus positive. As for showing that $\partial J_{\text{cycle}}/\partial \mathfrak{F}_{\text{edge}} = \partial^2 c/\partial \mathfrak{F}_{\text{edge}} \partial \mathfrak{F}_{\text{cycle}} > 0$, we denote the warehouse state as state 1 and get the tilted matrix:

$$\tilde{\mathbf{M}} = \begin{bmatrix} \mathfrak{F}_{\text{node}} - 2 & e^{\mathfrak{F}_{\text{d}} + \mathfrak{F}_{\text{cycle}}} + e^{\mathfrak{F}_{\text{r}}} \\ e^{\mathfrak{F}_{\text{d}} - \mathfrak{F}_{\text{cycle}}} + e^{\mathfrak{F}_{\text{r}}} & -2 \end{bmatrix}. \quad (43)$$

The caliber is the largest eigenvalue of $\tilde{\mathbf{M}}$:

$$c(\mathfrak{F}) = \frac{\sqrt{R} - (4 - \mathfrak{F}_{\text{node}})}{2} \quad (44)$$

where $R = (4 - \mathfrak{F}_{\text{node}})^2 - 8(2 - \mathfrak{F}_{\text{node}}) + 4(e^{\mathfrak{F}_{\text{d}} + \mathfrak{F}_{\text{cycle}}} + e^{\mathfrak{F}_{\text{r}}})(e^{\mathfrak{F}_{\text{d}} - \mathfrak{F}_{\text{cycle}}} + e^{\mathfrak{F}_{\text{r}}})$. We can then compute the desired $\partial J/\partial \mathfrak{F}_{\text{edge}} = \partial^2 c/\partial \mathfrak{F}_{\text{cycle}} \partial \mathfrak{F}_{\text{edge}}$. Due to the assumed symmetry, we can pick either $\mathfrak{F}_{\text{edge}} = \mathfrak{F}_{\text{d}}$ or \mathfrak{F}_{r} . Either way, a direct second derivative calculation will show that [41] $\partial J_{\text{cycle}}/\partial \mathfrak{F}_{\text{edge}} = J_{\text{cycle}}/2$, which is positive in our case here.

This example shows that to fully characterize the effect of a perturbation (here tuning f'), it is necessary to consider *all* the fundamental components of the dynamics— $(\pi_{\text{node}}, \tau_{\text{edge}}, J_{\text{cycle}})$ or $(\mathfrak{F}_{\text{node}}, \mathfrak{F}_{\text{edge}}, \mathfrak{F}_{\text{cycle}})$. The field of stochastic thermodynamics primarily focuses on $\pi_{\text{node}}, J_{\text{cycle}}$ and $\mathfrak{F}_{\text{cycle}}$ [4–7, 10] and is thus insufficient to derive conjugated relations to explain the opposite trends of J_{cycle} and $\mathfrak{F}_{\text{cycle}}$ in this example and other similar molecular-level examples [45]. We have demonstrated how the force coordinate in CFT can parse a transformation into perturbation in forces and restore conjugacy. All forces are needed for a complete analysis: not just the cycle forces.

Example 3. Observable-force coordinate characterizes the effect of traffic congestion.

We show here that CFT’s thermodynamic-like coordinate analysis can help characterize traffic congestion and the price of anarchy by considering a Markov process version of Pigou’s simple congestion game [46]. This example also demonstrates the usage of CFT’s fluctuation-susceptibility equalities in mixed observable-force coordinate.

Congestion in truck’s cargo delivery and reloading.

Consider a truck delivery company that has two warehouses near a city for cargo reload, as depicted in Fig. 4(a). Warehouse 1 reloads faster with a city re-enter rate r_1 for each truck (average reload time $1/r_1$) whereas warehouse 2 has a slower rate r_2 . Suppose the average delivery time of the city is $1/r_c$, and the truck driver has a probability ρ to choose to reload at warehouse 1. The long-term (normalized) total delivery flux is $\pi_c r_c = \pi_1 r_1 + \pi_2 r_2$ where (π_1, π_c, π_2) are the long-term distribution of trucks in warehouse 1, city, and warehouse 2. Further assume that warehouse 1 has a flux capacity limit K , say due to its finite number of reloading agents. When more truck chose warehouse 1 (bigger ρ), the delivery flux from warehouse 1, i.e. $\pi_1 r_1$, will saturate (decreasing r_1) and lead to congestion, as shown in Fig. 4(b).

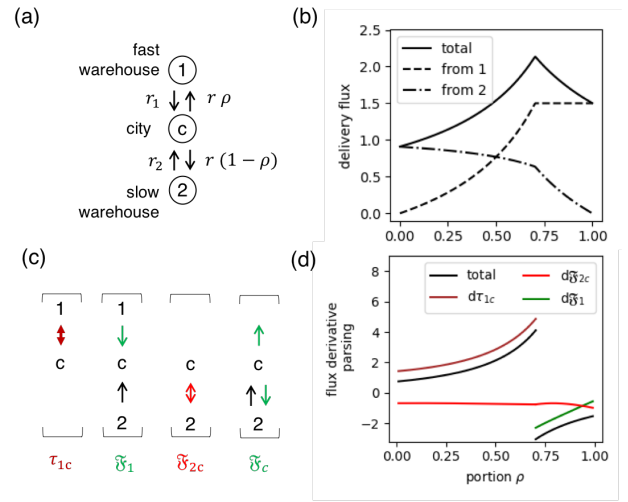


Figure 4. **Analyzing Traffic Congestion with CFT’s mixed observable-force coordinate.** (a) A Markov dynamics version of Pigou’s simple congestion game. Trucks can choose to reload their cargoes after delivering them to the city from two warehouses. The fast warehouse has a flux upper limit K . (b) When more truck chose to reload at the faster warehouse 1 (bigger ρ), it ultimately leads to a saturated delivery flux from warehouse 1 and a decreasing total delivery flux. (c) The CFT coordinate used to characterize the truck dynamics. τ_1 is the traffic through warehouse 1, \mathfrak{F}_1 is the node force 1, \mathfrak{F}_{2c} is the edge force through warehouse 2, and \mathfrak{F}_c is the node force of the city state. (d) Decomposition of deliver flux slope before and after the congestion. $d\tau_1$ represents the components from changing τ_1 , and likewise for $d\mathfrak{F}_{2c}$ and $d\mathfrak{F}_1$. Parameters used in this plot are $r_1 = r = 10$, $r_2 = 1$, and $K = 1.5$.

The minimum of r_1 happens when all trucks chose warehouse 1 ($r_1 = K$ when $\pi_1 = 1$). If this minimum is still bigger than the reload rate of the other warehouse $K > r_2$, then congestion will naturally happen if all truck drivers chose the faster warehouse (Nash “equilibrium”). This shows the price of anarchy. Fig. 4(b) shows that the maximal total delivery flux happens when a right portion of drivers use the slower warehouse 2—at the critical point when congestion happens.

Response Parsing with CFT’s force-observable coordinate. The Markov dynamics that describes each truck is four dimensional, and we can use CFT’s coordinate to characterize the effect of congestion. We use the mixed coordinate $\mathbf{z} = (\mathfrak{F}_1, \mathfrak{F}_c, \tau_{1c}, \mathfrak{F}_{2c})$ where $\mathfrak{F}_1 = r_2 - r_1$, $\mathfrak{F}_c = r_2 - r_c$, $\tau_{1c} = \pi_1 r_1 + \pi_c r_c \rho$ is the total traffic in and out of warehouse, and $\mathfrak{F}_{2c} = (1/2) \ln[r_2 r_c (1 - \rho)]$. This is a convenient coordinate because \mathfrak{F}_1 and \mathfrak{F}_c are fixed before the congestion happened whereas τ_{1c} and \mathfrak{F}_{2c} are fixed afterward. Since the total delivery flux is $\pi_c r_c$, and r_c is fixed at all times. We can focus on how ρ affects π_c and use CFT to parse the response before and after congestion into two elementary components:

$$\text{(before)} \quad \frac{d\pi_c}{d\rho} = \frac{\partial\pi_c}{\partial\tau_{1c}} \frac{\partial\tau_{1c}}{\partial\rho} + \frac{\partial\pi_c}{\partial\mathfrak{F}_{2c}} \frac{\partial\mathfrak{F}_{2c}}{\partial\rho}; \quad (45a)$$

$$\text{(after)} \quad \frac{d\pi_c}{d\rho} = \frac{\partial\pi_c}{\partial\mathfrak{F}_1} \frac{\partial\mathfrak{F}_1}{\partial\rho} + \frac{\partial\pi_c}{\partial\mathfrak{F}_{2c}} \frac{\partial\mathfrak{F}_{2c}}{\partial\rho}. \quad (45b)$$

These four terms (multiplied by r_c) are shown in Fig. 4(d). We see that the negative effect from \mathfrak{F}_{2c} (red curve) does not change much before and after the congestion. The dominant effect is, as expected, captured by switching from fixing \mathfrak{F}_1 (and increasing τ_{1c} , brown curve) before the congestion to fixing τ_{1c} (and increasing \mathfrak{F}_1 , green curve) afterward.

Relating Susceptibility to Spontaneous Fluctuation.

Here's how the four terms on the right of Eqs. (45) are computed. First, we can compute the $\partial z/\partial\rho$ terms with the rate expressions of z , which can be obtained after solving $(\pi_1, \pi_c, \pi_2) = (r_2 r_c \rho/D, r_1 r_2/D, r_1 r_c(1-\rho)/D)$ and $D = r_2 r_c \rho + r_1 r_2 + r_1 r_c(1-\rho)$ and how r_1 varies after the congestion. See [41] for details. The coefficients $\partial\pi_c/\partial z$, on the other hand, can be computed either by obtaining $\pi_c(z)$ or by relating these susceptibility terms to observable fluctuations. We demonstrate both methods here to illustrate our framework.

The coordinate z can be obtained from a (partial) Legendre transform from the force coordinate $\mathfrak{F} = (\mathfrak{F}_1, \mathfrak{F}_c, \mathfrak{F}_{1c}, \mathfrak{F}_{2c})$. The ‘‘thermodynamic-like’’ potential for coordinate z is

$$\phi(z) = \tau_{1c} \mathfrak{F}_{1c} - c(\mathfrak{F}). \quad (46)$$

The force \mathfrak{F}_{1c} is a function of z , solved by inverting $\tau_{1c} = \partial c/\partial\mathfrak{F}_{1c}$. After getting $\mathfrak{F}_{1c}(z)$, one can compute π_c via

$$\pi_c(z) = \frac{\partial c}{\partial\mathfrak{F}_c}[\mathfrak{F}_1, \mathfrak{F}_c, \mathfrak{F}_{1c}(z), \mathfrak{F}_{2c}] = -\frac{\partial\phi}{\partial\mathfrak{F}_c}(z) \quad (47)$$

where the last equality is a ‘‘thermodynamic-like’’ result from CFT derived by taking partial derivative of Eq. (46) with respect to \mathfrak{F}_c . Derivative of $\pi_c(z)$ can then be solved.

The second method of computing $\partial\pi_c/\partial z$ via fluctuation-susceptibility equalities are actually easier to implement numerically. Denoting the (co)variance term $V_{a,b} = \partial^2 c/\partial\mathfrak{F}_a\partial\mathfrak{F}_b$ where $\mathfrak{F}_a, \mathfrak{F}_b \in \mathfrak{F}$ and using our general result in Eqs. (24), we get the following fluctuation-susceptibility equalities in z :

$$\frac{\partial\pi_c}{\partial\tau_{1c}}(z) = \frac{V_{c,1c}}{V_{1c,1c}} \quad (48a)$$

$$\frac{\partial\pi_c}{\partial\mathfrak{F}_{2c}}(z) = V_{c,2c} - \frac{V_{c,1c}V_{1c,2c}}{V_{1c,1c}} \quad (48b)$$

$$\frac{\partial\pi_c}{\partial\mathfrak{F}_1}(z) = V_{c,1} - \frac{V_{c,1c}V_{1c,1}}{V_{1c,1c}}. \quad (48c)$$

Once we get the covariance matrix $V_{a,b}$ by inverting the Hessian of negative path entropy ($-\mathfrak{s}_{\text{path}}$), we can then compute all these susceptibility terms [41]. This is easier than

the first approach.

We show in this example how CFT uses mixed coordinate to give a ‘‘thermodynamic-like’’ analysis on traffic congestion. We illustrate how the congestion effect can be parsed into elementary dynamical components, how CFT identifies the dominant mechanism, and how CFT computes the system's dynamical responses and relates them to fluctuation.

Example 4: Speed and Accuracy Maximization under Energy Constraint

Molecular machines in biology often have a fixed source of energy that drives their nonequilibrium cycle flux, e.g. the free energy difference of ATP hydrolysis. The often-assumed idealized condition of fixed ‘‘waste and fuel’’ (ADP, Pi, and ATP) concentrations corresponds to a fixed level of cycle force in CFT (a fixed cycle affinity in the language of ST). A evolutionary optimization problem for these molecular machines is then how to maximize the cycle flux (average speed) [47–49] and/or minimize its fluctuation [50–52] given the cycle force energy constraint. Universal tradeoff relations among speed, accuracy, and energy cost—known as the thermodynamic uncertainty relation (TUR) [19, 38]—have been derived, but not much is known about the principles to approach the optimal. Here, we show that CFT can provide the observable-based coordinate to parameterize the remaining degrees of freedom given the energy constraint and help reveal principles to optimize molecular machine performance. We consider the simplest unicircular example here for illustration and leave more thorough exploration and multicircular generalizations for future studies.

Average Speed Maximization with fixed Cycle Force.

Here, we follow [47] and consider a two-state-two-edge model for molecular motors, which has a four-dimensional phase space. Mathematically, this is the same model as the truck delivery model in Example 2 with the delivery (return) edge replaced by the chemical (mechanical) edge of ATP binding (mechanical stepping), c.f. Fig. 3(a) and Fig. 5(a). Using Eq. (38), the cycle force can be expressed and rewritten in the observable coordinate as the following:

$$\mathfrak{F}_{\text{cycle}} = \frac{1}{2} \ln \left[\frac{\tau_c + J}{\tau_c - J} \cdot \frac{\tau_m + J}{\tau_m - J} \right] \quad (49a)$$

$$= \frac{1}{2} \ln \left[\frac{\rho + \frac{J}{\tau_{\text{tot}}}}{\rho - \frac{J}{\tau_{\text{tot}}}} \cdot \frac{(1-\rho) + \frac{J}{\tau_{\text{tot}}}}{(1-\rho) - \frac{J}{\tau_{\text{tot}}}} \right] \quad (49b)$$

where τ_c, τ_m are the traffic levels on the chemical and mechanical edges, $\tau_{\text{tot}} = \tau_c + \tau_m$ is the total traffic across the cycle and $\rho = \tau_m/\tau_{\text{tot}}$ is the traffic distribution. The cycle flux can then be solved in the form of

$$J = \tau_{\text{tot}} G(\rho, \mathfrak{F}_{\text{cycle}}) \quad (50)$$

where $G(\rho, \mathfrak{F}) = \coth(\mathfrak{F})/2 - \sqrt{\dots}/[4 \sinh(\mathfrak{F})]$ and

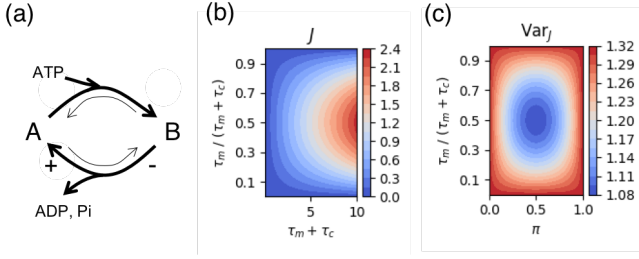


Figure 5. Speed and Fluctuation Optimization of Molecular Motors under fixed Chemical Energy Source. (a) shows the state space of a two-state molecular motor driven by ATP hydrolysis. Upper edge is the chemical energy input step of binding of ATP, and the lower edge is the output step of mechanical forward stepping accompanied by ADP and Pi release. All transitions (thin arrows) are invertible. (b) shows the levels of average cycle flux J in the phase space of processes with fixed cycle force. τ_c is the traffic on the upper chemical edge whereas τ_m is the traffic on the lower mechanical edge. (c) shows the fluctuation of cycle flux Var_J for processes with fixed average flux J and cycle force. π is the steady-state probability of state A. For illustration simplicity, we set $\mathfrak{F}_{\text{cycle}} = 1$ in (b) and (c) and $J = 1$ in (c).

$\sqrt{\dots} = \sqrt{2 + 8\rho(1 - \rho) + 2(1 - 2\rho)^2 \cosh(2\mathfrak{F})}$ ². This shows that, under the mixed coordinate $(\pi, \tau_c, \tau_m, \mathfrak{F}_{\text{cycle}})$ and when $\mathfrak{F}_{\text{cycle}}$ is fixed, increasing τ_{tot} scales up the cycle flux whereas J is maximized when the traffic distribution is uniform $\rho = 1/2$. See Fig. 5(b) for illustration. CFT tells us that this optimal is degenerate: we can freely tune the state distribution π (probability of being at state A) to arrive various processes with the same J and $\mathfrak{F}_{\text{cycle}}$ (and $\rho = 1/2$).

Flux Fluctuation Minimization with fixed Average Flux and Cycle Force. TUR describes the tradeoff among average cycle flux J , long-term scaled fluctuation of cycle flux V_J (second derivative of the caliber), and the cycle force $\mathfrak{F}_{\text{cycle}}$. For unicyclic processes, it simplifies to

$$\frac{V_J}{J} \geq \frac{1}{\mathfrak{F}_{\text{cycle}}}. \quad (51)$$

Here we show how CFT provides the coordinate to parameterize the phase space of processes constrained on fixed cycle force $\mathfrak{F}_{\text{cycle}}$ and cycle flux J and reveal principles for the constrained minimization of the cycle flux fluctuation V_J .

The CFT coordinate $(\pi, \tau_c, \tau_m, \mathfrak{F}_{\text{cycle}})$ can be easily rewritten in terms of the traffic distribution and total traffic, $(\pi, \rho, \tau_{\text{tot}}, \mathfrak{F}_{\text{cycle}})$. Then, by using Eq. (50), we can get a new coordinate $(\pi, \rho, J, \mathfrak{F}_{\text{cycle}})$ useful for exploring the performance of the molecular motor under speed J and cycle force $\mathfrak{F}_{\text{cycle}}$ constraints. Here, we compute V_J by the second derivative of the caliber in Eq. (44), which can be reduced to the

following form in this simple example³:

$$\frac{V_J}{J} = \coth(\mathfrak{F}_{\text{cycle}}) - 4\pi(1 - \pi) G(\rho, \mathfrak{F}_{\text{cycle}}). \quad (52)$$

The minimization of V_J under fixed J and $\mathfrak{F}_{\text{cycle}}$ can then be carried out by varying state probability π and traffic ratio ρ . In this simple example, the minimization is achieved when $\pi = 1/2$ and $\rho = 1/2$, leading to a rotational symmetric process—consistent with known result [38]. The power of CFT is in two-fold: (1) it provides the coordinates for the to-be-optimized degrees of freedom (here π and ρ); (2) the observable-based coordinate can facilitate further calculation, if there are additional observable constraints. For example, myosin is known to spend small time fraction attach to the actin [53, 54], a constraint on $\pi \rightarrow 1$ for myosin described by this two-state model. Calculations above show that V_J is maximized by a uniform traffic distribution under the additional $\pi \approx 1$ constraint. This uniform-traffic rule of thumb is a testable prediction from CFT.

This simple example demonstrates how CFT helps analyze constrained optimization problems for NEQ processes, relevant in studying the constrained optimization that evolution might seek to solve for biochemical processes [55] or molecular machines [47–49].

Example 5. Generalizing Circuit Theory for Stochastic Transport in Networks

There are two Kirchoff Laws of transport on networks, often applied to electrical circuits: (1) Kirchoff’s Current Law, which says that the sum of (net) currents into a node equals the sum of currents out of the node, and (2) Kirchoff’s Voltage Law, which says that the voltage differences around a circuit must sum to zero. CFT gives new insight here, and shows that there is a third such law, which comes from the third network force; namely edge forces. Kirchoff’s laws are essentially macroscale, effectively neglecting any fluctuational back traffic, for example as would appear in few-particle transport problems. Kirchoff’s two laws neglect the back and forth flows along edges, which, following Maes, we have called “traffic” here [36]. The third Kirchoff-like law pertains when the back-and-forth flows along edges are relevant, such as in few-particle few-vehicle situations.

Consider the simple networks shown in Fig. 6(a,b) with resource particles diffusing in chambers (nodes) connected by various channels (edges). These networks composed of chambers and channels can serve as the state space of resource particles consumed by different sets of agents in a well-mixed tank. We consider two cases here. The first case in Fig. 6a

² This kind of rewriting can be done for any unicyclic processes. It’s just that the function G is in general numerically solved for state number larger than 2 or 3.

³ First, we compute V_J as a function of the forces. Then, forces can be expressed in terms of the transition rates, which can be expressed in terms of $\pi, \rho, \mathfrak{F}_{\text{cycle}}$ and $G(\rho, \mathfrak{F}_{\text{cycle}})$. See Supplemental Material for more details.

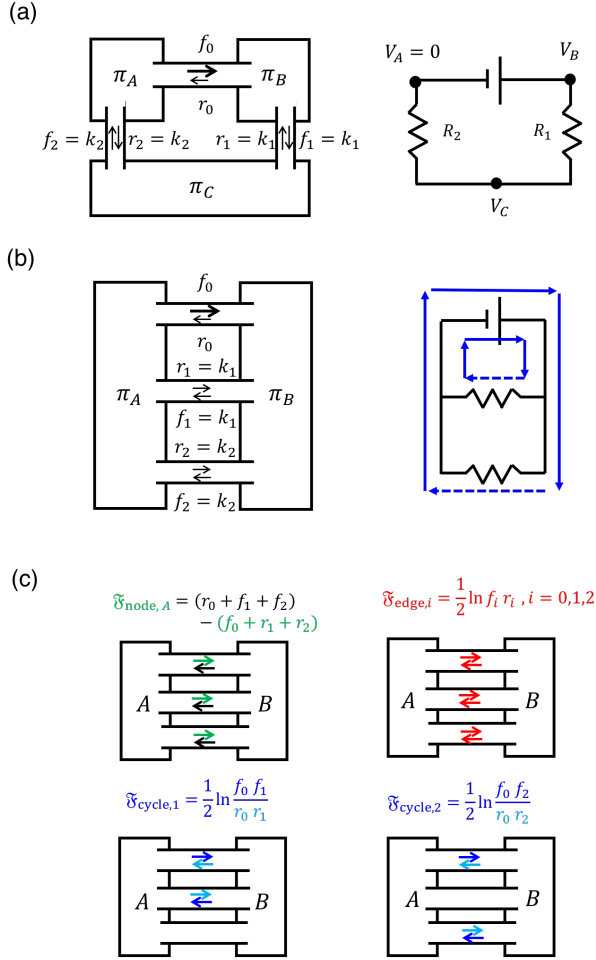
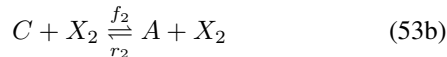
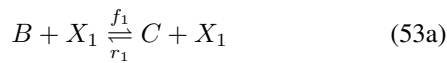


Figure 6. **Network state space of resource particles consumed by agents working in series or in parallel.** (a) shows a case where agents work in series like an electric circuit with one battery and two resistor. The top edge has a forward and backward per particle flow rate given by f_0 and $r_0 (< f_0)$. The other edges are symmetric $f_i = r_i = k_i$. (b) shows a case where the two agents compete for the same resources. The two cycles in blues on the right depict the two fundamental cycle fluxes that span all edge fluxes. The dashed edges are the defining edges of the two fundamental cycles. The edge flux on the defining edge determines the level of the fundamental cycle flux. The top edge has two fundamental cycles went through, so the edge flux there is the sum of the two fundamental cycle fluxes. (c) shows the forces in the parallel channel case in (b).

is an scenario where an usable resource B is consumed by agents X_1 and X_2 in sequence, and then recycled by the environment. These are described by three chemical-like reactions forming a cycle for the resource particles:

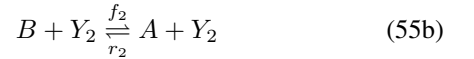


Here, reaction rates, as the (posterior) Markov transition rates in CFT, are defined empirically as the ratio of flux and distribution of a resource particle in different states (A, B, C) in the long-trajectory limit $L \rightarrow \infty$. For example,

$$f_0 = \lim_{L \rightarrow \infty} \frac{\# \text{ of } A \mapsto B}{\text{total time in } A}, \quad (54)$$

which is essentially the inverse of the average waiting time for an A to be converted to a B . Throughout this example, recycling are assumed to be efficient $f_0 > r_0$.

The second case in Fig. 6b is a scenario where two agents Y_1 and Y_2 compete for the same type of resources, consuming the resource in parallel:



These two cases describe toy scenarios of more general resource allocation problems for organs/systems consuming/competing the same resource.

Kirchhoff's two laws apply to symmetric pipes. We first consider symmetric agents X and Y modeled by equal forward and backward reaction rates $f_i = r_i = k_i, i = 1, 2$. We can show that these agents satisfy Kirchhoff's laws and Ohm's law with the difference in the distribution π as voltage, the net flux J as current and $1/k_i$ as the resistance. For agents in series in Fig. 6a, we have

$$J = \frac{\pi_B - \pi_C}{1/k_1} = \frac{\pi_C - \pi_A}{1/k_2} = \frac{\pi_B - \pi_A}{1/k_1 + 1/k_2}. \quad (56)$$

On the other hand, for agents in parallel, the net fluxes through the three edges (J_0 to the right and J_1, J_2 to the left) satisfy

$$\frac{J_1}{J_2} = \frac{k_1}{k_2} \text{ and } J_0 = J_1 + J_2 = (\pi_B - \pi_A)(k_1 + k_2). \quad (57)$$

These Markov-process-analogy of Kirchhoff's and Ohm's laws are known [56, 57], and they rely on the symmetry of rates $f_i = r_i = k_i$. If the agents have asymmetry rates $f_i \neq r_i$, the relations between net flux J and distribution difference $\Delta\pi$ are more complicated, and CFT gives the principled details in those cases.

With asymmetric pipes, edge traffic forces also contribute to generalized conductance. Consider asymmetric rates $f_i > r_i, i = 1, 2$ in Fig. 6b. The traffic τ_i and net flux J_i through the two agents can be solved using Markov dynamic, but expressing them in terms of the forces also gives the governing laws.

The flow ratio, J_1/J_2 , has the following form based on the edge and cycle forces [41]:

$$\frac{J_1}{J_2} = \frac{e^{\mathfrak{F}_{edge,1}}}{e^{\mathfrak{F}_{edge,2}}} \times (\text{ratio 1 in all } \mathfrak{F}_{edge} \text{ and } \mathfrak{F}_{cycle}). \quad (58)$$

Now, consider a special case where the two agents are asymmetric at the same level $f_1 = f_2 > r_1 = r_2$, i.e. the two channels carry the same types of “batteries”. Then, the cycle forces are the same: $\mathfrak{F}_{\text{cycle},1} = \mathfrak{F}_{\text{cycle},2} = (1/2)[\ln(f/r) + \ln(f_1/r_1)]$. In such a case, Eq. (58) reduces to splitting the fluxes based on the ratio of exponential edge forces,

$$\frac{J_1}{J_2} = \frac{e^{\mathfrak{F}_{\text{edge},1}}}{e^{\mathfrak{F}_{\text{edge},2}}} = \frac{\sqrt{f_1 r_1}}{\sqrt{f_2 r_2}}, \quad (59)$$

telling us that the exponential of the edge force on the right $\sqrt{f_i r_i}$ is the generalized conductance for $f_i \neq r_i$. The ratio 1 on the right of Eq. (58) is the effect of the two competing agents Y_1 and Y_2 having different cycle forces $\mathfrak{F}_{\text{cycle},1} \neq \mathfrak{F}_{\text{cycle},2}$ (specific form shown in [41]).

The allocation of traffic terms also support identifying exponential edge forces as generalized conductance. With detailed calculation shown in [41], we compute the traffic ratios of the three parallel channels:

$$\frac{\tau_0}{\tau_1} = \frac{e^{\mathfrak{F}_{\text{edge},0}}}{e^{\mathfrak{F}_{\text{edge},1}}} \times (\text{ratio 2 in all } \mathfrak{F}_{\text{edge}} \text{ and } \mathfrak{F}_{\text{cycle}}) \quad (60a)$$

$$\frac{\tau_2}{\tau_1} = \frac{e^{\mathfrak{F}_{\text{edge},2}}}{e^{\mathfrak{F}_{\text{edge},1}}} \times (\text{ratio 3 in all } \mathfrak{F}_{\text{edge}} \text{ and } \mathfrak{F}_{\text{cycle}}). \quad (60b)$$

Further insight comes from looking at two special cases. First, when all cycle forces are zero, it is a EQ system (like three resistors connected in parallel) with detailed balanced steady state. The traffic on the three channels in parallel are directly proportional to the conductance defined by the exponential of edge forces:

$$\tau_0 : \tau_1 : \tau_2 = e^{\mathfrak{F}_{\text{edge},0}} : e^{\mathfrak{F}_{\text{edge},1}} : e^{\mathfrak{F}_{\text{edge},2}}. \quad (61)$$

Second, when the system is nonequilibrium but with equal cycle force $\mathfrak{F}_{\text{cycle},1} = \mathfrak{F}_{\text{cycle},2} > 0$ so the two cycle force effects are symmetric, the traffic ratio of channel 1 and 2 is, as the net flux ratio J_1/J_2 , determined by the edge forces

$$\frac{\tau_1}{\tau_2} = \frac{e^{\mathfrak{F}_{\text{edge},1}}}{e^{\mathfrak{F}_{\text{edge},2}}} = \frac{\sqrt{f_1 r_1}}{\sqrt{f_2 r_2}}. \quad (62)$$

Ratios 2 and 3 on the right of Eqs. (60) are again corrections for asymmetric cycle forces.

These results add to Kirchhoff’s current and voltage principles when fluctuations are important. They show how the net flux allocates based on edge forces in a multicircular network. CFT can also be applied to asymmetric pipes in series as in Fig. 6a or more complicated networks. This example shows how CFT can reveal new principles of network flows.

DISCUSSION

Here, we add some context. First, Max Cal is relevant to dynamics in two different ways. In the same sense that the state entropy in EQ thermodynamics can apply either to

inferring microscopic distribution functions from models, or as a macroscopic force quantity that is conjugate to energy, Max Cal also has microscopic and macroscopic purposes. Max Cal is useful for model-making as a principle that gives self-consistent inferences about pathway distributions, given a dynamical model [13–15, 58–61]. For different values of the constrained observables, the posterior predicted models form a Boltzmann-like exponential family of path probabilities, a subset of the full phase space. But, here we focus instead on Max Cal as a force principle conjugated to flow variables. We exploit Max Cal’s conjugate relations between the constrained observables and the Lagrange multipliers to *derive coordinates* and *analyze the phase space of processes* with the same state space. We need Max Cal to cover the full phase space. Hence, we consider the idealized situation where all relevant degrees of freedom are non-degenerate within a set of observables, prescribed by our First-Law-like principle.

Second, we note that while LDT is generally understood as a framework for computing rare-event statistics under the deterministic limit of stochastic models [37, 62, 63], LDT can also be used to identify force parameters [24, 27, 64]. This latter usage is equivalent to Max Cal (or Maximum Entropy) inference [24–27, 59, 65]. Our contribution here is to also harness the First-Law-like principle to ensure that the posterior models cover the full phase space. This has an important consequence. While the Lagrange multipliers in prior efforts can be hard to interpret, requiring numerical solution, CFT shows that, in our First-Law-like framing, the conjugated multipliers have *analytical* expressions in terms of the transition rates. So, they are meaningfully interpretable in terms of the dynamics. That is a key for connecting LDT and Max Cal to ST, deriving the conjugated relations between cycle flux and cycle force.

Finally, we note an interesting relationship between path entropies and EPR. It has been shown in ST that the steady-state time irreversibility is essentially the relative entropy between a NEQ process and its *dual* (the process with reversed steady-state net cycle flux) [8, 66–68]:

$$\text{EPR} = \lim_{L \rightarrow \infty} \frac{1}{L} \sum_{i_{0:L}} P[i_{0:L}] \ln \frac{P[i_{0:L}]}{P^\dagger[i_{0:L}]} \quad (63)$$

where P^\dagger is the path probability of the dual process. CFT makes the meaning of the dual process clearer by providing a coordinate: a process with $(\pi_{\text{node}}, \tau_{\text{edge}}, J_{\text{cycle}})$ has a dual process with $(\pi_{\text{node}}, \tau_{\text{edge}}, -J_{\text{cycle}})$. From this, it can be shown that the steady-state time irreversibility is the (posterior) path entropy difference:

$$\text{EPR} = \mathfrak{s}_{\text{path}}^\dagger - \mathfrak{s}_{\text{path}}. \quad (64)$$

This reveals an interesting structure of the phase space among the *doldrum state* (reference process of the path entropy), the process, and the dual of the process, as well as the operators that change one to another [68].

ACKNOWLEDGMENTS

We thank the Laufer center for support, and the anonymous reviewer, Yuhai Tu, Jonathan Pachter, Charles Kocher, Olga

Movilla Miangolarra, Rostam Razban, Lakshmanji Verma, and Jin Wang for insightful feedback. Y.-J. expresses his deepest gratitude to Hong Qian for guiding him in learning the essential theoretical pieces used in the present work.

-
- [1] See companion paper at [URL] for derivation and more backgrounds.
- [2] C. Gardiner, *Stochastic Methods: A Handbook for the Natural and Social Sciences*, 4th ed., Springer Series in Synergetics (Springer-Verlag, Berlin Heidelberg, 2009).
- [3] N. G. V. Kampen, *Stochastic Processes in Physics and Chemistry*, 3rd ed. (North Holland, Amsterdam ; Boston, 2007).
- [4] J. Schnakenberg, Network theory of microscopic and macroscopic behavior of master equation systems, *Rev. Mod. Phys.* **48**, 571 (1976).
- [5] T. L. Hill, *Free Energy Transduction and Biochemical Cycle Kinetics* (Springer-Verlag, New York, 1989).
- [6] U. Seifert, Stochastic thermodynamics: From principles to the cost of precision, *Physica A: Statistical Mechanics and its Applications* **504**, 176 (2018).
- [7] C. Van den Broeck and M. Esposito, Ensemble and trajectory thermodynamics: A brief introduction, *Physica A: Statistical Mechanics and its Applications Proceedings of the 13th International Summer School on Fundamental Problems in Statistical Physics*, **418**, 6 (2015).
- [8] D.-Q. Jiang, M. Qian, and M.-P. Qian, *Mathematical Theory of Nonequilibrium Steady States: On the Frontier of Probability and Dynamical Systems*, 2004th ed. (Springer, Berlin ; New York, 2004).
- [9] H. Qian, S. Kjelstrup, A. B. Kolomeisky, and D. Bedeaux, Entropy production in mesoscopic stochastic thermodynamics: nonequilibrium kinetic cycles driven by chemical potentials, temperatures, and mechanical forces, *J. Phys.: Condens. Matter* **28**, 153004 (2016).
- [10] Y.-J. Yang and H. Qian, Bivectorial Nonequilibrium Thermodynamics: Cycle Affinity, Vorticity Potential, and Onsager's Principle, *J Stat Phys* **182**, 46 (2021).
- [11] J. A. Owen, T. R. Gingrich, and J. M. Horowitz, Universal Thermodynamic Bounds on Nonequilibrium Response with Biochemical Applications, *Phys. Rev. X* **10**, 011066 (2020).
- [12] T. Aslyamov and M. Esposito, Nonequilibrium Response for Markov Jump Processes: Exact Results and Tight Bounds, *Phys. Rev. Lett.* **132**, 037101 (2024).
- [13] E. T. Jaynes, The Minimum Entropy Production Principle, *Annual Review of Physical Chemistry* **31**, 579 (1980).
- [14] S. Pressé, K. Ghosh, J. Lee, and K. A. Dill, Principles of maximum entropy and maximum caliber in statistical physics, *Rev. Mod. Phys.* **85**, 1115 (2013).
- [15] S. Davis, D. González, and G. Gutiérrez, Probabilistic Inference for Dynamical Systems, *Entropy* **20**, 696 (2018), number: 9 Publisher: Multidisciplinary Digital Publishing Institute.
- [16] J. A. Pachter, Y.-J. Yang, and K. A. Dill, Entropy, irreversibility and inference at the foundations of statistical physics, *Nat Rev Phys*, 1 (2024).
- [17] C. Jarzynski, Equalities and Inequalities: Irreversibility and the Second Law of Thermodynamics at the Nanoscale, *Annual Review of Condensed Matter Physics* **2**, 329 (2011).
- [18] U. Seifert, From Stochastic Thermodynamics to Thermodynamic Inference, *Annual Review of Condensed Matter Physics* **10**, 171 (2019).
- [19] J. M. Horowitz and T. R. Gingrich, Thermodynamic uncertainty relations constrain non-equilibrium fluctuations, *Nat Phys* **16**, 15 (2020).
- [20] H. Qian and H. Ge, *Stochastic Chemical Reaction Systems in Biology*, 1st ed. (Springer, Switzerland, Cham, 2021).
- [21] L. Peliti and S. Pigolotti, *Stochastic Thermodynamics: An Introduction* (Princeton University Press, 2021).
- [22] M. Vellela and H. Qian, Stochastic dynamics and non-equilibrium thermodynamics of a bistable chemical system: the Schlögl model revisited, *Journal of The Royal Society Interface* **6**, 925 (2008).
- [23] L. M. Martyushev and V. D. Seleznev, The restrictions of the maximum entropy production principle, *Physica A: Statistical Mechanics and its Applications* **410**, 17 (2014).
- [24] R. Chetrite and H. Touchette, Nonequilibrium Microcanonical and Canonical Ensembles and Their Equivalence, *Phys. Rev. Lett.* **111**, 120601 (2013).
- [25] R. Chetrite and H. Touchette, Nonequilibrium Markov Processes Conditioned on Large Deviations, *Ann. Henri Poincaré* **16**, 2005 (2015).
- [26] R. Chetrite and H. Touchette, Variational and optimal control representations of conditioned and driven processes, *J. Stat. Mech.* **2015**, P12001 (2015).
- [27] Y.-J. Yang and H. Qian, Statistical uncertainty principle in Markov kinetics, *Annals of Physics* **469**, 169780 (2024).
- [28] K. Huang, *Statistical Mechanics, 2nd Edition*, 2nd ed. (Wiley, New York, 1987).
- [29] L. Onsager and S. Machlup, Fluctuations and Irreversible Processes, *Phys. Rev.* **91**, 1505 (1953).
- [30] L. D. Landau and E. M. Lifshitz, *Statistical Physics, Third Edition, Part 1: Volume 5*, 3rd ed. (Butterworth-Heinemann, Amsterdam u.a, 1980).
- [31] A. Dechant and S.-i. Sasa, Fluctuation–response inequality out of equilibrium, *Proceedings of the National Academy of Sciences* **117**, 6430 (2020), publisher: Proceedings of the National Academy of Sciences.
- [32] K. Ptaszyński, T. Aslyamov, and M. Esposito, Dissipation Bounds Precision of Current Response to Kinetic Perturbations, *Phys. Rev. Lett.* **133**, 227101 (2024), publisher: American Physical Society.
- [33] M. Baiesi, C. Maes, and B. Wynants, Fluctuations and Response of Nonequilibrium States, *Phys. Rev. Lett.* **103**, 010602 (2009).
- [34] B. Altaner, M. Poletini, and M. Esposito, Fluctuation-Dissipation Relations Far from Equilibrium, *Phys. Rev. Lett.* **117**, 180601 (2016).
- [35] G. Fernandes Martins and J. M. Horowitz, Topologically constrained fluctuations and thermodynamics regulate nonequilibrium response, *Phys. Rev. E* **108**, 044113 (2023).
- [36] C. Maes, Frenesy: Time-symmetric dynamical activity in nonequilibrium, *Physics Reports* **850**, 1 (2020).
- [37] H. Touchette, The large deviation approach to statistical mechanics, *Physics Reports* **478**, 1 (2009).

- [38] A. C. Barato and U. Seifert, Thermodynamic Uncertainty Relation for Biomolecular Processes, *Phys. Rev. Lett.* **114**, 158101 (2015).
- [39] Z. Koza, General technique of calculating the drift velocity and diffusion coefficient in arbitrary periodic systems, *J. Phys. A: Math. Gen.* **32**, 7637 (1999).
- [40] R. T. Rockafellar, *Convex Analysis* (Princeton University Press, 1970).
- [41] See Supplemental Material at [URL] for derivations and more details.
- [42] A. C. Barato and U. Seifert, Dispersion for two classes of random variables: General theory and application to inference of an external ligand concentration by a cell, *Phys. Rev. E* **92**, 032127 (2015).
- [43] H. C. Berg and E. M. Purcell, Physics of chemoreception, *Biophysical Journal* **20**, 193 (1977).
- [44] R. G. Endres and N. S. Wingreen, Maximum Likelihood and the Single Receptor, *Phys. Rev. Lett.* **103**, 158101 (2009), publisher: American Physical Society.
- [45] M. Baiesi and C. Maes, Life efficiency does not always increase with the dissipation rate, *J. Phys. Commun.* **2**, 045017 (2018).
- [46] A. Pigou, *The Economics of Welfare*, 2013th ed. (Palgrave Macmillan, Houndmills, Basingstoke, Hampshire ; New York, 2013).
- [47] J. A. Wagoner and K. A. Dill, Mechanisms for achieving high speed and efficiency in biomolecular machines, *PNAS* **116**, 5902 (2019).
- [48] J. A. Wagoner and K. A. Dill, Evolution of mechanical cooperativity among myosin II motors, *Proc. Natl. Acad. Sci. U.S.A.* **118**, e2101871118 (2021).
- [49] A. I. Brown and D. A. Sivak, Theory of Nonequilibrium Free Energy Transduction by Molecular Machines, *Chem. Rev.* **120**, 434 (2020).
- [50] G. Lan, P. Sartori, S. Neumann, V. Sourjik, and Y. Tu, The energy-speed-accuracy tradeoff in sensory adaptation, *Nat Phys* **8**, 422 (2012).
- [51] Y. Cao, H. Wang, Q. Ouyang, and Y. Tu, The free-energy cost of accurate biochemical oscillations, *Nature Phys* **11**, 772 (2015).
- [52] A. C. Barato and U. Seifert, Cost and Precision of Brownian Clocks, *Phys. Rev. X* **6**, 041053 (2016).
- [53] B. Alberts, A. Johnson, J. Lewis, M. Raff, K. Roberts, and P. Walter, *Molecular Motors*, *Molecular Biology of the Cell*. 4th edition (2002).
- [54] G. Piazzesi, M. Reconditi, M. Linari, L. Lucii, P. Bianco, E. Brunello, V. Decostre, A. Stewart, D. B. Gore, T. C. Irving, M. Irving, and V. Lombardi, Skeletal Muscle Performance Determined by Modulation of Number of Myosin Motors Rather Than Motor Force or Stroke Size, *Cell* **131**, 784 (2007).
- [55] A. Cornish-Bowden, *Biochemical Evolution: The Pursuit of Perfection*, 2nd ed. (Garland Science, New York, 2016).
- [56] M. M. Lin, Circuit Reduction of Heterogeneous Nonequilibrium Systems, *Phys. Rev. Lett.* **125**, 218101 (2020).
- [57] J. A. Pachter, K. A. Dill, J. K. Sodhi, and L. Z. Benet, Review of the application of Kirchhoff's Laws of series and parallel flows to pharmacology: Defining organ clearance, *Pharmacology & Therapeutics* **239**, 108278 (2022).
- [58] J. Shore and R. Johnson, Axiomatic derivation of the principle of maximum entropy and the principle of minimum cross-entropy, *IEEE Trans. Inf. Theor.* **26**, 26 (1980).
- [59] I. Csiszar, T. Cover, and Byoung-Seon Choi, Conditional limit theorems under Markov conditioning, *IEEE Trans. Inform. Theory* **33**, 788 (1987).
- [60] S. Pressé, K. Ghosh, J. Lee, and K. A. Dill, Nonadditive Entropies Yield Probability Distributions with Biases not Warranted by the Data, *Phys. Rev. Lett.* **111**, 180604 (2013).
- [61] A. Caticha, Entropy, Information, and the Updating of Probabilities, *Entropy* **23**, 895 (2021).
- [62] A. C. Barato and R. Chetrite, A Formal View on Level 2.5 Large Deviations and Fluctuation Relations, *J Stat Phys* **160**, 1154 (2015).
- [63] L. Bertini, A. De Sole, D. Gabrielli, G. Jona-Lasinio, and C. Landim, Macroscopic fluctuation theory, *Rev. Mod. Phys.* **87**, 593 (2015), publisher: American Physical Society.
- [64] C. Maes and K. Netočný, Canonical structure of dynamical fluctuations in mesoscopic nonequilibrium steady states, *EPL* **82**, 30003 (2008).
- [65] J. van Campenhout and T. Cover, Maximum entropy and conditional probability, *IEEE Trans. Inform. Theory* **27**, 483 (1981).
- [66] M. Esposito and C. Van den Broeck, Three Detailed Fluctuation Theorems, *Phys. Rev. Lett.* **104**, 10.1103/PhysRevLett.104.090601 (2010).
- [67] U. Seifert, Stochastic thermodynamics, fluctuation theorems and molecular machines, *Rep. Prog. Phys.* **75**, 126001 (2012).
- [68] Y.-J. Yang and H. Qian, Unified formalism for entropy production and fluctuation relations, *Phys. Rev. E* **101**, 022129 (2020).